Electronic Supplementary Information

Ammonium Ion Pre-Intercalation Stabilized Tunnel *h*-WO_3 for Fast NH_4^+ Storage

Qiang Chen,[a] Mengda Song,[a] Xiangyong Zhang,[c] Jiangli Zhang,[a] Guangya Hou, [a] and Yiping Tang,*[a]

[a] College of Material Science and Engineering, Zhejiang University of Technology, Hangzhou 310014, China.

[b] College of Material Science and Engineering, Shenzhen University, Shenzhen 30035, China. E-mail: tangyiping@zjut.edu.cn (Y. Tang); E-mail: yd_deng@hainanu.edu.cn (Y. Deng)

Experimental Section

***Synthesis of $(NH_4)_xWO_3$ nanorods anode*:** $(NH_4)_xWO_3$ nanorods grown on carbon cloth (CC) were obtained via a simple hydrothermal method. The CC (2 cm × 3 cm) was firstly cleaned with ethanol, DI water in ultrasonic machine, and then dried at 80 °C oven. 12.5 mmol $Na_2WO_4{\cdot}2H_2O$ was dissolved in 100 ml DI water, after stirring the vigorously solution for 30 mins, then add 3.0 M HCl to the above solution and adjust the pH to 1.2. 35 mmol (4.41 g) of $H_2C_2O_4$ was dissolved in the above mixed solution and the solution was diluted to 250 ml to form a H_2WO_4 solution. Transfer 80 ml of the obtained precursor solution (H_2WO_4) and the pretreated CC to a Teflon-lined stainless steel autoclave (100 ml) and add 4 g of $(NH_4)_2SO_4$. The sealed autoclave was heated to 180 °C for 20 h. The samples washed with DI water several times, and dried. The mass loading of the $(NH_4)_xWO_3$ measured to be 19.1 mg cm^{-2}. The synthesis of *h*-WO_3 and $WO_3{\cdot}0.33(H_2O)$ is similar to $(NH_4)_xWO_3$, except that the addition amount of the precursor liquid $(NH_4)_2SO_4$ is 1 and 0 g, respectively. The mass loading of the *h*-WO_3 and $WO_3{\cdot}0.33(H_2O)$ were measured to be 23.1 and 26.1 mg cm^{-2}, respectively.

***Synthesis of α-MnO_2* nanowires *cathode*:** 1.26 g $KMnO_4$ was dissolved distilled water (75 ml), and then added 2 ml 98% H_2SO_4 into the solution. After stirring for 15 min, the CC and the resultant precursor solution moved to a Teflon-lined stainless-steel autoclave (100 ml). The sealed autoclave was heated to 140

°C for 2.5 h. The samples washed with DI water several times, and dried. The mass loading of the α-MnO_2 cathode measured to be 15.5 mg cm^{-2}.

***Materials Characterizations*:** X-ray diffraction (XRD, Rigaku D/Max 2550 PC) was employed to characterize the crystalline structures. The morphology and microstructure of the as-prepared materials were demonstrated by a field-emission SEM (FEI Nani SEM450) and TEM (Tecnai G2 F30 S-Twin), HRTEM, HAADF-STEM, EDS (RUKER EDS QUANTAX). The valence states of elements were detected by an XPS (EscaLab 250Xi). Raman spectrum tests were characterized by Renishaw InVia Raman microscopy system. Fourier transform infrared spectroscopy was conducted by a Fourier transform infrared spectrometer (FT-IR, Thermo Fisher Nicolet, Nicolet6700, America). The Brunauer Emmett Teller (BET) surface area was measured with an ASAP 2020M (Micromeritics Instrument Corp.).

***Electrochemical Measurements*:** The electrochemical measurements were collected on an electrochemical workstation (CHI 760D). In the three-electrode system, $(NH_4)_xWO_3$ nanorods were used as the working electrode, a Pt tablets was used as the counter electrode, and saturated calomel electrode (SCE) served as the reference electrode in a 2.0 M NH_4Ac electrolyte. The electrochemical performances of the aqueous $(NH_4)_xWO_3$//α-MnO_2 A-HSC were studied in a two-electrode system in a solution of 2.0 M NH_4Ac.

Calculations:

The areal capacitances (C_a) of electrodes were measured by galvanostatic discharge method using the following equation:

$$C_a = \frac{I \times \Delta t}{\Delta V \cdot S} \quad (1)$$

where I (mA) is the constant discharging current, Δt (s) is the discharging time, and S (cm^2) is the area of electrodes.

The areal energy density (E_a, μWh cm^{-2}) and power density (P_a, mW cm^{-2}) of the Zn-HSCs were

obtained from the following equations:

$$E_a = 1/2 \times C_a \times (\triangle V)^2 \times 10^6 \quad (2)$$

$$P_a = E_a/\triangle t \times 3600 \times 10^{-3} \quad (3)$$

where $\triangle V$ is the discharging voltage range (1.8 V), and $\triangle t$ is the discharge time (s).

Balance the charge of electrodes in A-HSCs device:

As for a SC, the charge balance will follow the relationship $q^+ = q^-$. The charge stored by each electrode depends on the capacitance (C_a), the potential range for the charge/discharge process (ΔE) and the area of the electrode (A). It follows the Equation (4):

$$q = C_a \times \Delta E \times m \quad (4)$$

In order to get $q^+ = q^-$ at 8 mA cm^{-2}, the area balancing between α-MnO_2 and $(NH_4)_xWO_3$ electrode will be calculated as follow (5):

$$\frac{A_{\alpha-MnO2}}{A_{(NH4)xWO3}} = \frac{C_{A((NH4)xWO3)} \times \Delta E_{((NH4)xWO3)}}{C_{A(\alpha-MnO2)} \times \Delta E_{(\alpha-MnO2)}} \approx \frac{1}{1} \quad (5)$$

The calculated $C_{A((NH4)xWO3)}$ is 5.69 F cm^{-2}, $\Delta E_{((NH4)xWO3)}$ is 1.0 V, $C_{A(\alpha\text{-MnO2})}$ is 5.63 F cm^{-2}, $\Delta E_{(\alpha\text{-MnO2})}$ is 1.0 V. Therefore, the calculated areal ratio between the α-MnO_2 electrode and $(NH_4)_xWO_3$ electrode is about 1 ： 1.

First-principles calculations were carried out using spin-polarized density functional theory (DFT) with generalized gradient approximation (GGA) of Perdew-Burke-Ernzerhof (PBE) implemented in the Vienna Ab-Initio Simulation Package (VASP).[S1, S2] The valence electronic states were expanded based on plane waves with the core-valence interaction represented using the projector augmented plane wave (PAW) approach[S3] and a cutoff of 450 eV. A Γ-centered k-mesh of 4 × 4 × 4 was used for bulk calculations. Convergence is achieved when the forces acting on ions become smaller than 0.02 eV/Å.

The adsorption energy is calculated as formula (6):

$$E_{ads} = E_{substrate+molecule} - E_{substrate} - E_{molecule} \quad (6)$$

where $E_{substrate+molecule}$, $E_{substrate}$, and $E_{molecule}$ are the total energies of the whole system, the substrate, and the gas phase molecule, respectively.

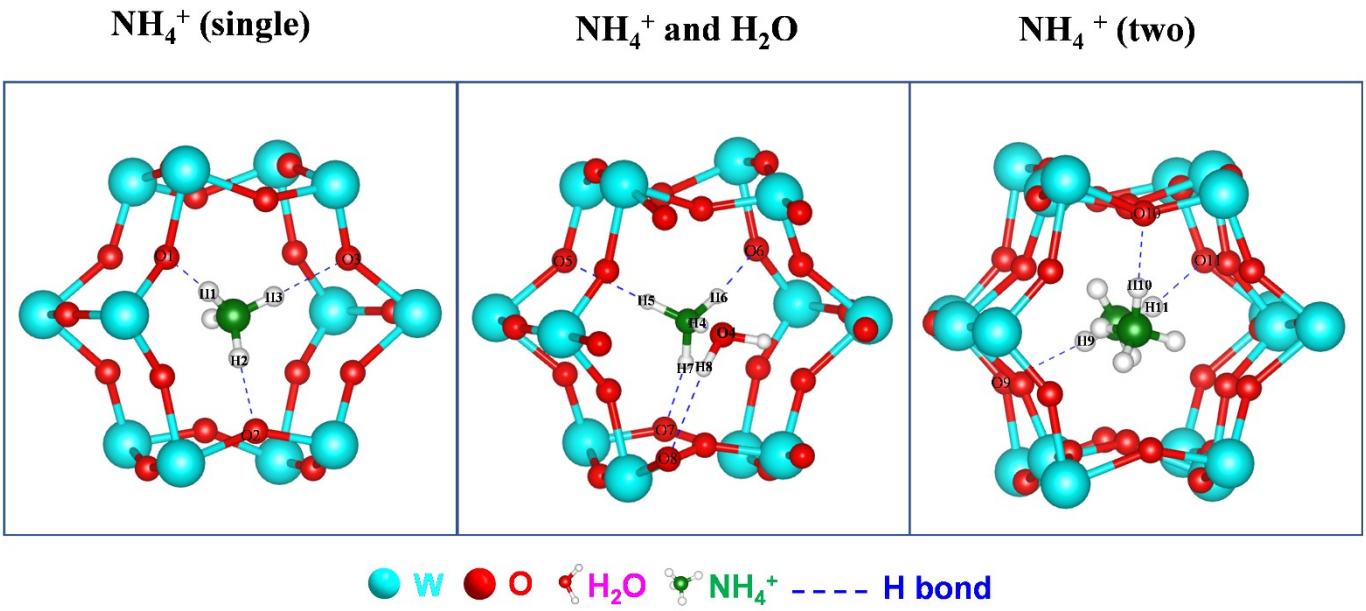

Fig. S1. The lower-energy model structure of NH_4^+ and H_2O intercalated WO_3.

Tab. S1. The calculated bond length of H bonds in NH_4^+ inserted $(NH_4)_xWO_3$ structure shown in Fig. S1.

Atoms	H Bond	Length (Å)
O (from WO_3)	O1-H1	1.888
H (from NH_4^+)	O2-H2	1.885
□	O3-H3	1.968
O (from H_2O) H (from NH_4^+)	O4-H4	1.772
O (from WO_3)	O5-H5	2.039
H (from NH_4^+)	O6-H6	1.832
	O7-H7	2.063

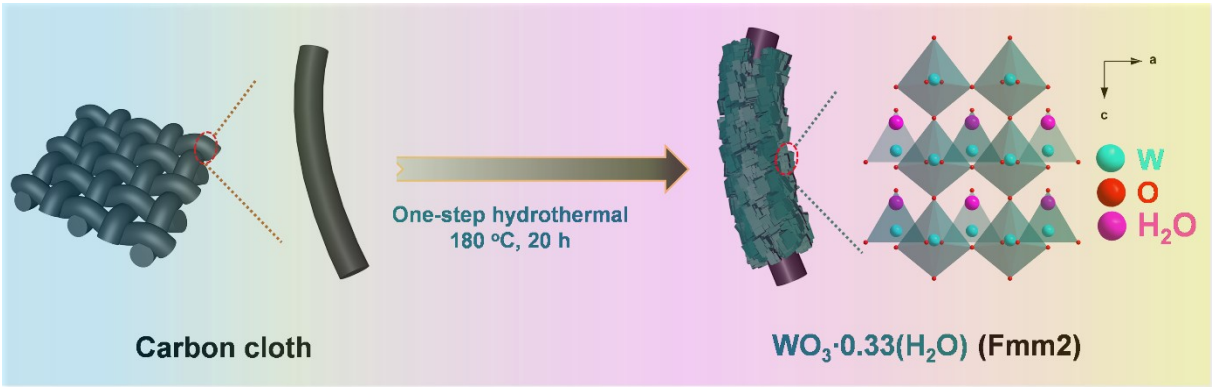

Fig. S2. Schematic illustration of the synthesis procedure of the $WO_3 \cdot 0.33(H_2O)$.

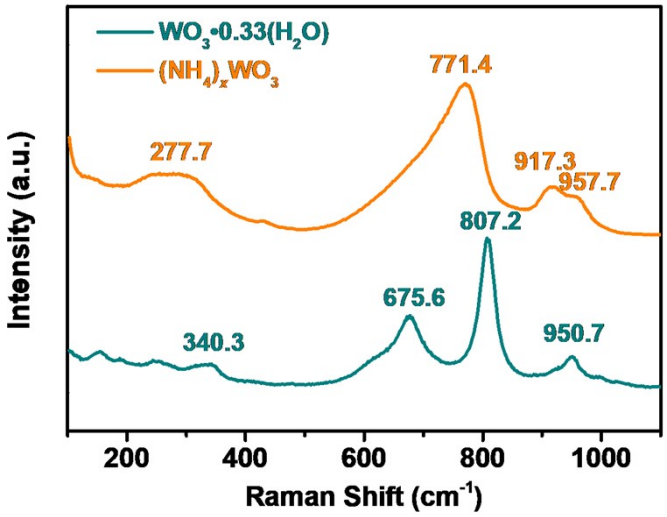

Fig. S3. Raman spectra of the $WO_3 \cdot 0.33(H_2O)$ and $(NH_4)_xWO_3$.

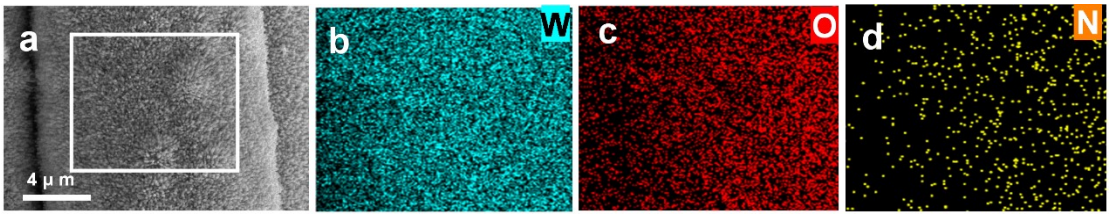

Fig. S4. SEM element mapping of the $(NH_4)_xWO_3$.

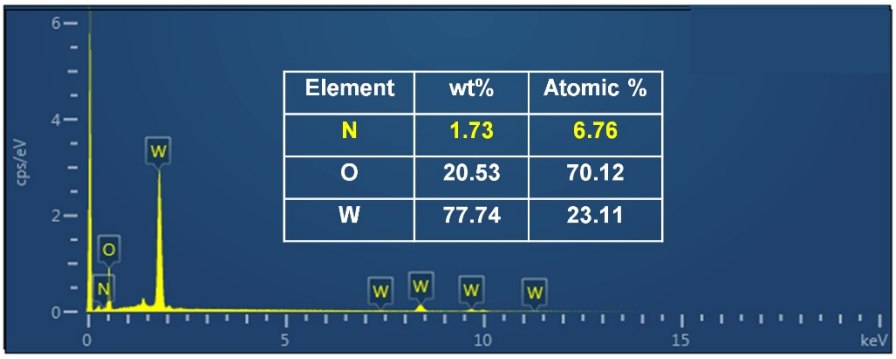

Fig. S5. EDS spectra of $(NH_4)_xWO_3$.

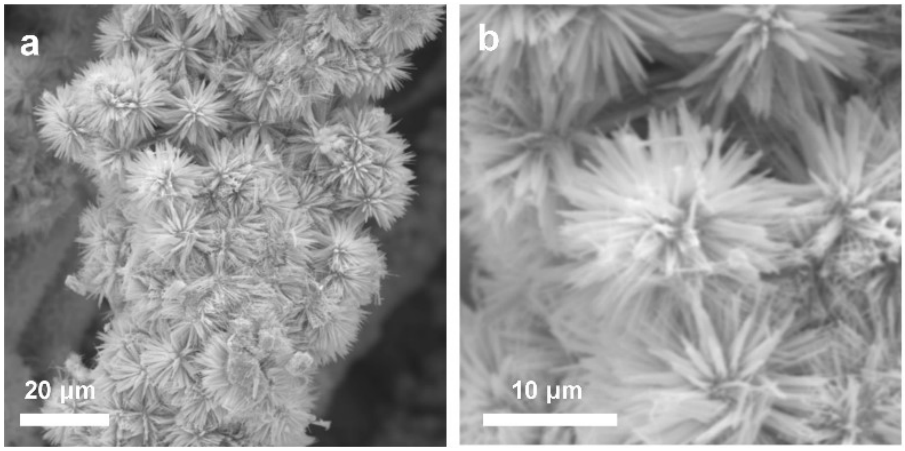

Fig. S6. SEM image of *h*-WO_3 at different magnifications.

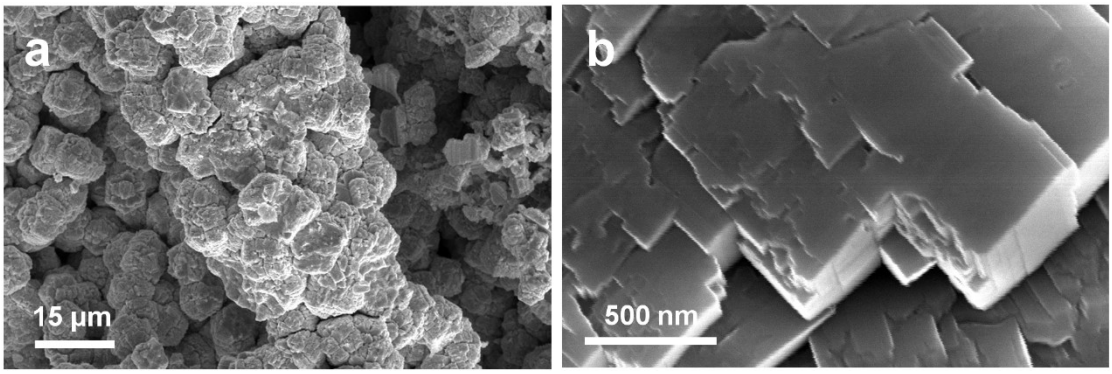

Fig. S7. SEM images of $WO_3 \cdot 0.33(H_2O)$ at different magnification.

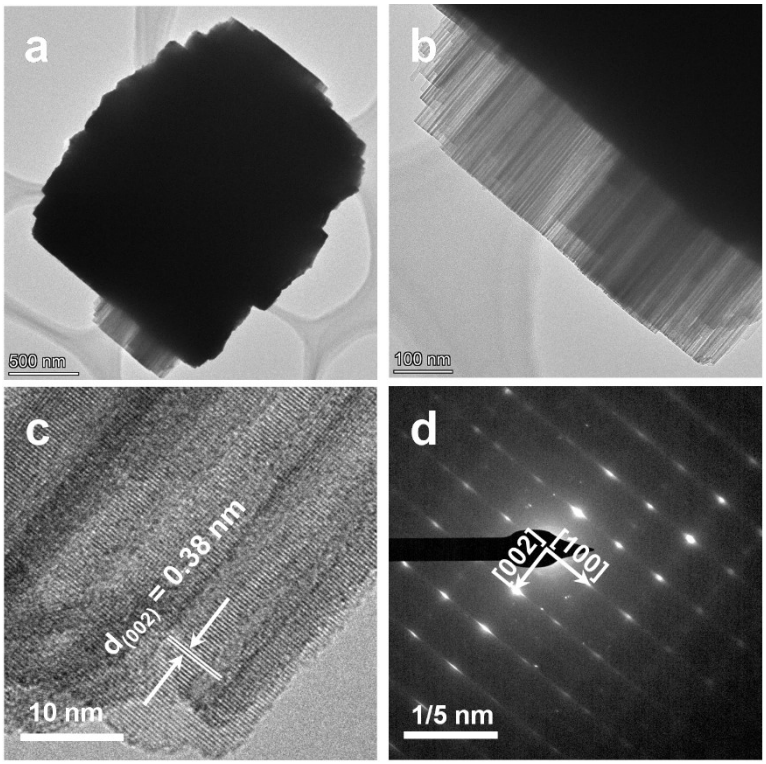

Fig. S8. (a, b) TEM, (b) HRTEM, and (d) SAED of the $WO_3 \cdot 0.33(H_2O)$.

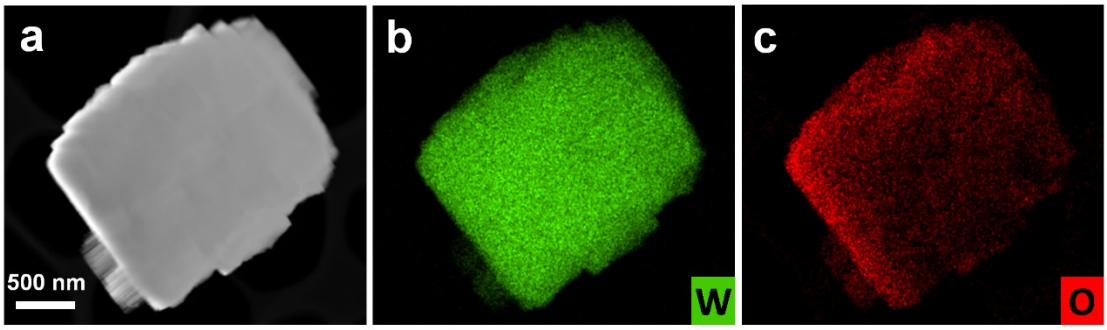

Fig. S9. TEM element mapping of the $WO_3 \cdot 0.33(H_2O)$.

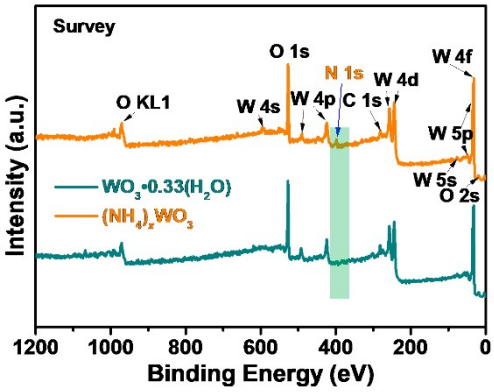

Fig. S10. XPS survey spectra of $WO_3 \cdot 0.33(H_2O)$ and $(NH_4)_xWO_3$.

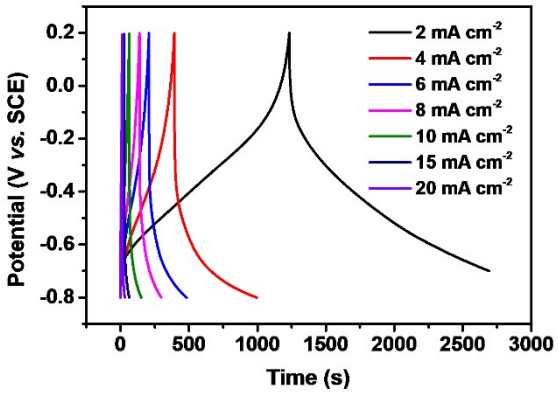

Fig. S11. GCD curves collected at different current density and scan rate of the $WO_3 \cdot 0.33(H_2O)$.

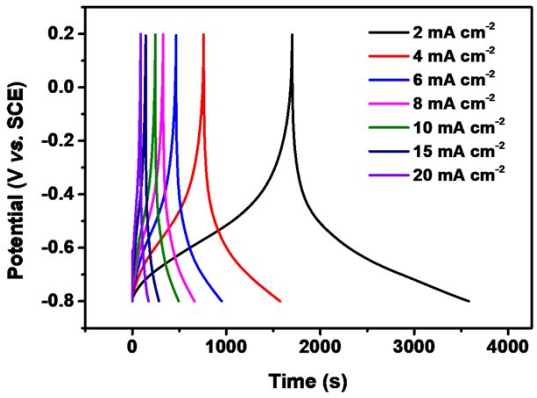

Fig. S12. GCD curves collected at different current density and scan rate of the *h*-WO_3.

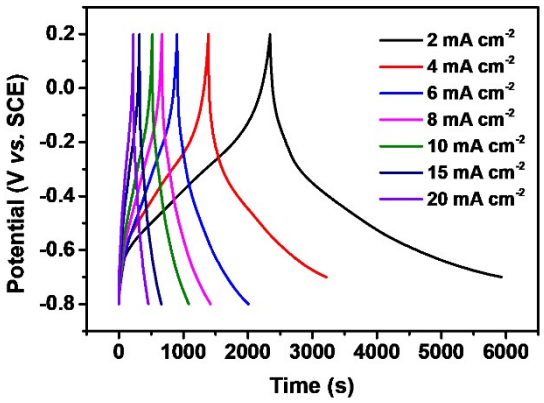

Fig. S13. GCD curves collected at different current density and scan rate of the $(NH_4)_xWO_3$.

Tab. S2. Comparison of the capacity performance of $(NH_4)_xWO_3$ to several recently reported supercapacitors.

Electrode	Substrate	Voltage Window [V]	Current density) [mA cm^{-2}]	GCD areal capacitance [F cm^{-2}]	Electrolyte	Reference
$(NH_4)_xWO_3$	CC	-0.8 - 0.2	2	8.0	2.0 M $(NH_4)Ac$	This work
$WO_3 \cdot 0.33H_2O$	CC	-0.8 - 0.2	2	3.3	2.0 M $(NH_4)Ac$	This work
$Na_{0.5}MnO_2$	CC	0.0 - 1.3	1	0.37	1.0 M Na_2SO_4	*Adv. Mater.* 2017, **29**, 1700804
δ-MnO_2	CC	0.0 - 1.0	2	6.8	1.0 M $(NH_4)_2SO_4$	*Adv. Mater.* 2021, 10.1002/adma.202107992
Zn_xMnO_2	CC	0.0 - 1.0	2	1.75	2 M $ZnSO_4$ + 0.4 M $MnSO_4$	*Small*, 2020, **16**, 2000091.
Phosphate ion functionalized-Co_3O_4	CC	-0.2 – 0.4	2.52	0.96	6.0 M KOH	*Adv. Mater.*, 2017, **29**, 1604167
NiO	NF	0.0 – 0.45	8	2.02	1.0 M KOH	*J. Mater. Chem. A*, 2018, **6**, 19488-19494.
Co-Ni_3S_2	NF	0.0 – 0.45	8	3.6	1.0 M KOH	*J. Mater. Chem. A*, 2020, **8**, 13114-13120.
WS_2	CC	-1.0 – 0.0	4	0.93	5 M LiCl	*J. Mater. Chem. A*, 2017, **5**, 21460-21466.
WO_{3-x}	CC	-1.0 – 0.0	1	1.83	5 M LiCl	*Electrochimica Acta* 2018, **283**, 639-645.

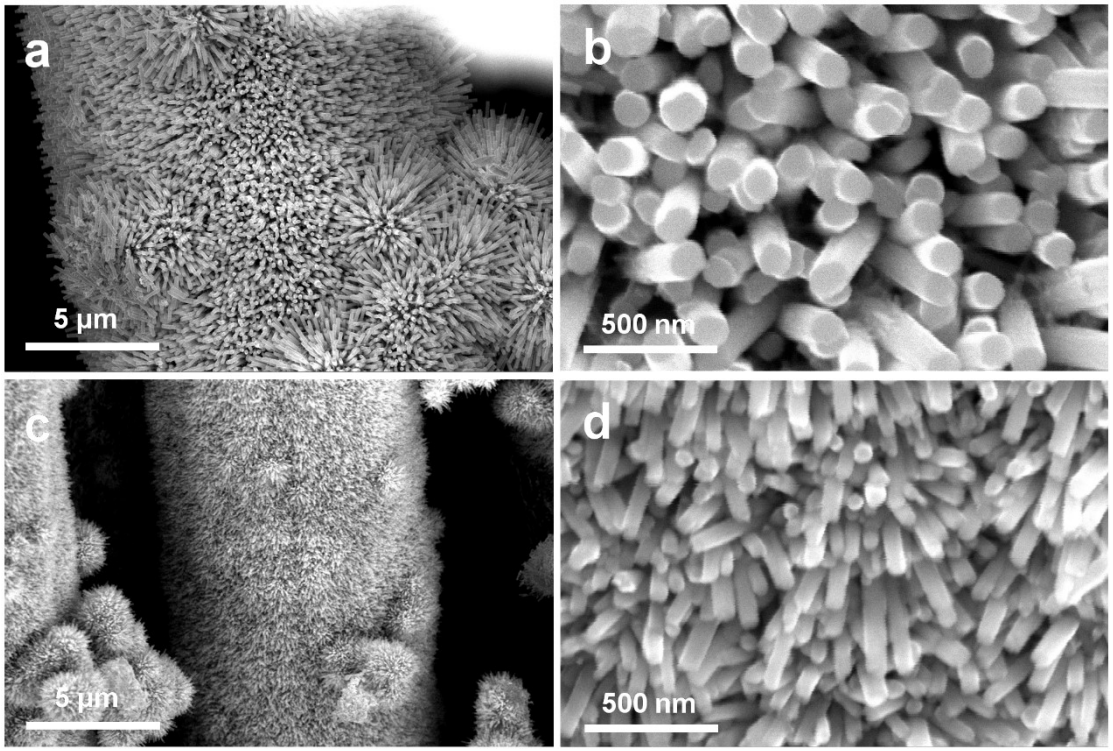

Fig. S14. SEM images of $(NH_4)_xWO_3$ samples with different $(NH_4)_2SO_4$ feeding amount: (a, b) 2 g, and (c, d) 6 g.

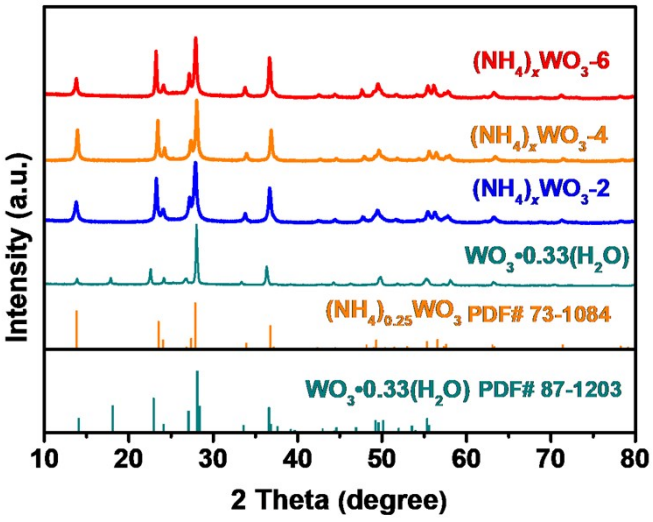

Fig. S15. XRD patterns of the $(NH_4)_xWO_3$ samples prepared with different $(NH_4)_2SO_4$ feeding amount.

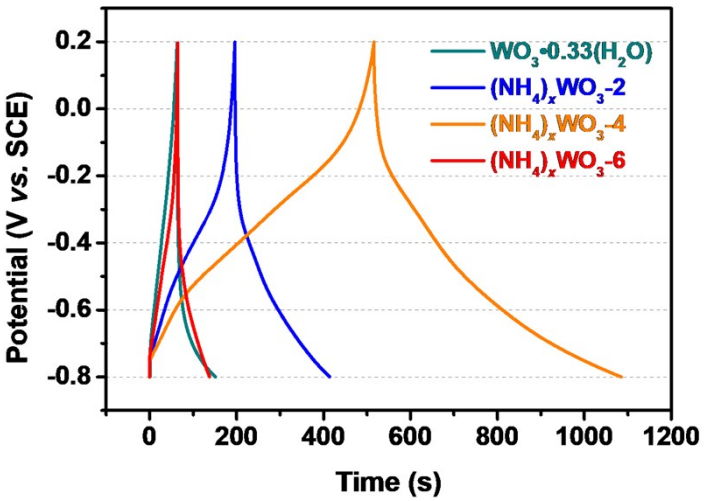

Fig. S16. GCD curves of the $(NH_4)_xWO_3$ samples prepared with different $(NH_4)_2SO_4$ feeding amount.

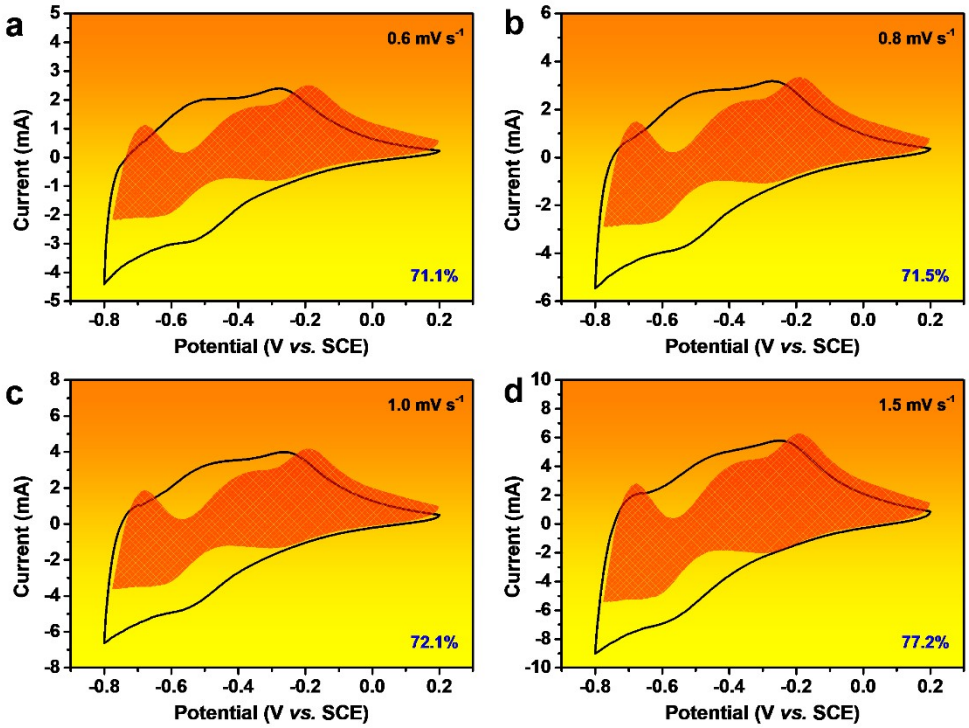

Fig. S17. Pseudo-capacitance contribution at scan rates of 0.6 - 1.5 mV s^{-1} for the $(NH_4)_xWO_3$ anode.

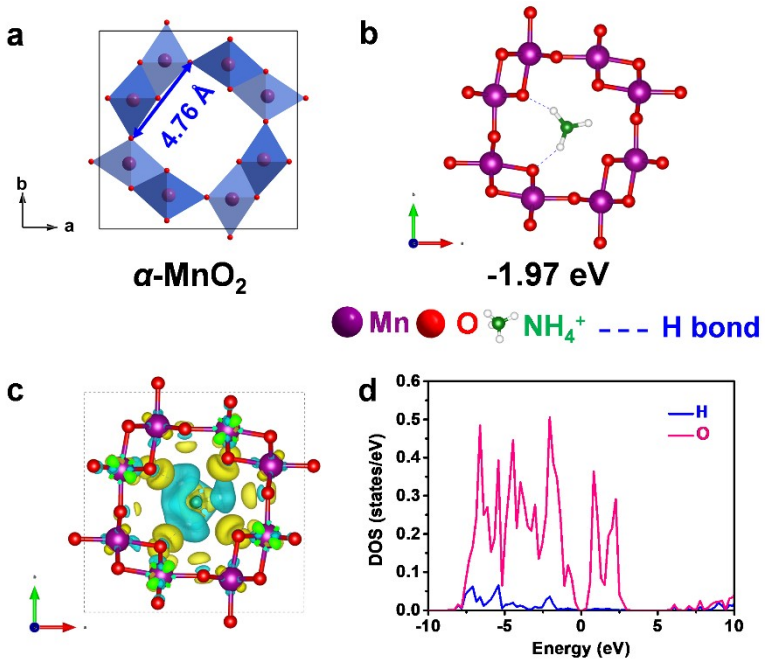

Fig. S18. (a) The crystal structure of the α-MnO_2. (b) Schematic diagram of the bond state and adsorption energy of a single NH_4^+ intercalated MnO_2 tunnel structure. (c) Diagram of charge density difference of NH_4^+ inserted tunnel structure α-MnO_2, where the charge density isosurfaces are 0.001 eÅ^{-3} for blue and 0.001 eÅ^{-3} for yellow. (d) The PDOS of H and O that form hydrogen bonds.

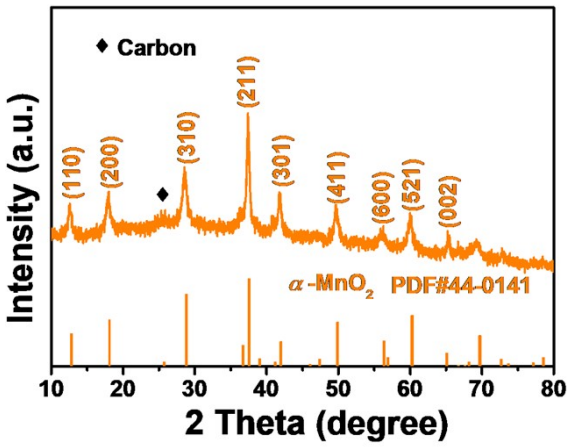

Fig. S19. XRD patterns of the α-MnO_2.

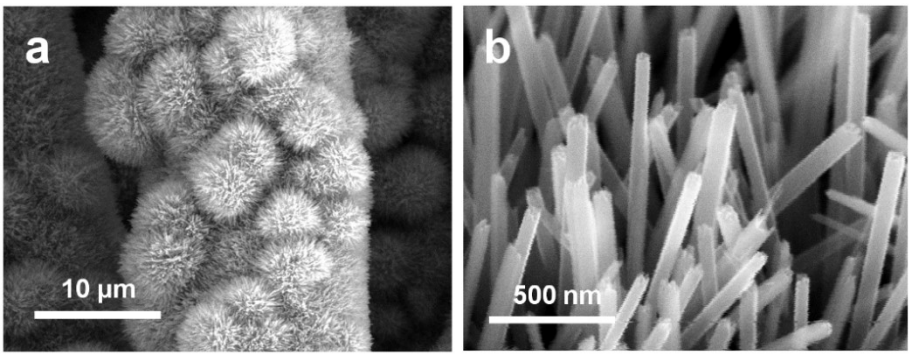

Fig. S20. SEM images of the α-MnO_2.

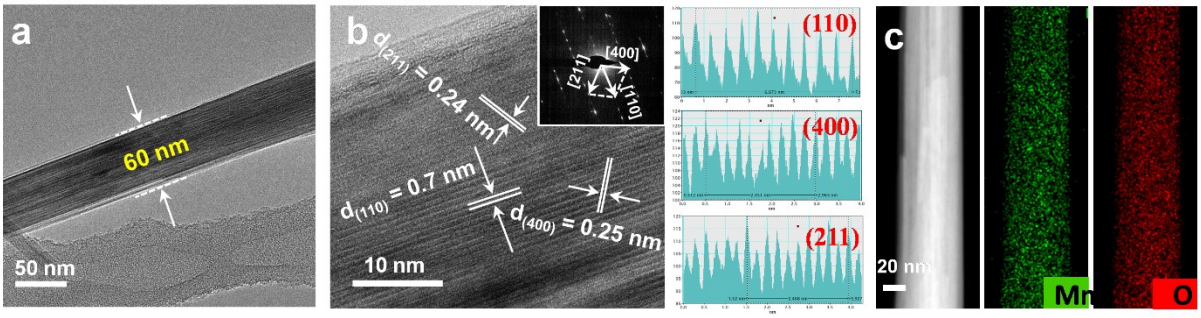

Fig. S21. (a) TEM image, (b) HRTEM, SAED (the inset), and (c) element mapping of the α-MnO_2.

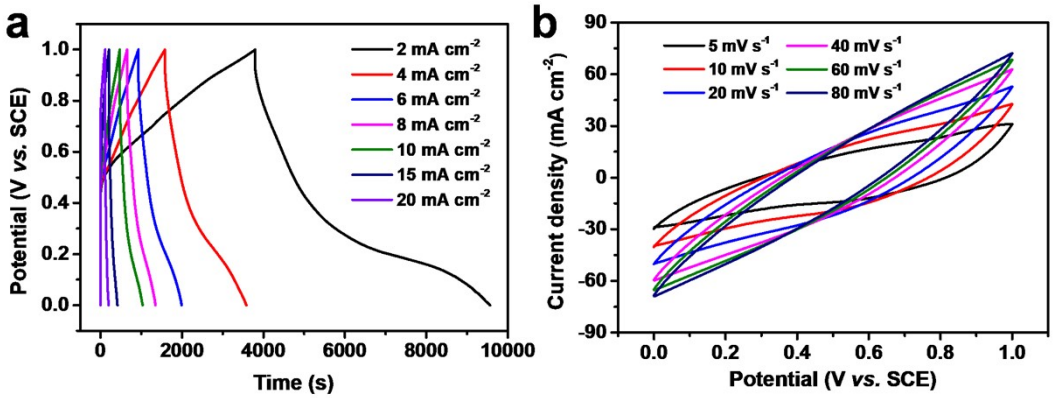

Fig. S22. (a) GCD and (b) CV curves collected at different current density and scan rate of the α-MnO_2 cathode.

Tab. S3. Comparison of the capacity performance and energy density of $(NH_4)_xWO_3$//α-MnO_2 to several recently reported supercapacitors.

Cathode	Anode	Current density) [mA cm^{-2}]	GCD areal capacitance [mF cm^{-2}]	Voltage Window [V]	Energy density [µWh cm^{-2}]	Electrolyte	Reference
α-MnO_2 [a]	$(NH_4)_xWO_3$	2	2239.7	0 – 1.8	1010.1	2.0 M $(NH_4)Ac$	This work
Zn_xMnO_2 [b]	ACC [c]	2	1745.8	0 – 2.0	969.9	2.0 M $ZnSO_4$ + 0.4 M $MnSO_4$	*Small* 2020, **16**, 2000091.
AC [b]	Zn foil [c]	0.16	1297	0.5 - 1.5	115.4	2.0 M $ZnSO_4$	*Adv. Mater.* 2019, **31**, 1806005.
Carbon nanotube [b]	Zn nanoflakes [c]	1	83.2	0.2 - 1.8	29.6	1.0 M $ZnSO_4$	*Energy Environ. Sci.* 2018, **11**, 3367.
G@PANI [b]	Zn foil [c]	0.2	874	0 – 0.8	410	2.0 M $ZnSO_4$	*Nanoscale* 2018, **10**, 13083.
AC [b]	Zn foil [c]	0.08	217.8	0.2 - 1.8	67.2	2.0 M $ZnSO_4$	*Energy Storage Mater.* 2018, **13**, 96.
GaN/MnO_2/MnON [c]	G/M/M [d]	0.1	1915.5	0 - 1.0	61	6.0 M KOH	*J. Mater. Chem. A* 2018, **6**, 13215.
CoHCF [c]	AC [d]	4.5	351	0 – 2.0	191.25	0.5 M Na_2SO_4	*Nano Energy* 2017, **39**, 647.

[a] A-HSCs; [b] Zn-HSCs [c] HSCs

References

[S1] Kresse G G , J.J. Furthmüller. *Phys. Rev. B: Condens. Matter.* **1996**, *54*, 11169.

[S2] Perdew JP, Burke K, Ernzerhof. M. *Phys. Rev. Lett.* **1998**, *77*, 3865.

[S3] Blochl. *Phys.Rev. B: Condens. Matter.* **1994**, *50*, 179539.